I&EC research
Industrial & Engineering Chemistry Research

Article

pubs.acs.org/IECR

Secondary Oil Recovery Using Graphene-Based Amphiphilic Janus Nanosheet Fluid at an Ultralow Concentration

Dan Luo,[†,‡,§] Feng Wang,[†] Jingyi Zhu,[§] Lu Tang,[†] Zhuan Zhu,[∥] Jiming Bao,[∥] Richard C. Willson,[‡,⊥] Zhaozhong Yang,[*,§] and Zhifeng Ren[*,†]

[†]Department of Physics and TcSUH, University of Houston, Houston, Texas 77204, United States

[‡]Department of Chemical and Biomolecular Engineering, University of Houston, Houston, Texas 77204, United States

[§]State Key Laboratory of Oil and Gas Reservoir Geology and Exploitation, Southwest Petroleum University, Chengdu, Sichuan 610500, China

[∥]Department of Electrical and Computer Engineering, University of Houston, Houston, Texas 77204, United States

[⊥]Tecnologico de Monterrey, Departamento de Biotecnologıa e Ingenierıa de Alimentos, Monterrey, Nuevo Leon 64849, Mexico

Supporting Information

ABSTRACT: Nanofluid of graphene-based amphiphilic Janus nanosheets produced high-efficiency tertiary oil recovery at a very low concentration (0.01 wt %). The more attractive way is to use nanofluid during the secondary oil recovery stage, which can eliminate the tertiary stage and save huge amounts of water, especially at times when the price of oil is low. Here, we continue to report our findings on the application of the same nanosheets in secondary oil recovery, which increased oil recovery efficiency by ≤7.5% at an ultralow concentration (0.005 wt %). Compared with nanofluids of homogeneous nanoparticles, our nanofluid achieved a higher efficiency at a much lower concentration. The nanosize dimension of this two-dimensional carbon material improves transport in rock pores. After single-side surface hydrophobization of oxidized graphene with alkylamine, the partial restoration of the graphitic sp^2 network was detected by Raman, ultraviolet−visible, etc. The amphiphilic Janus nature of nanosheets led to their unique behavior at toluene−brine interface. Oil immersion testing clearly showed the change in the shape of the droplet. The three-phase contact angle decreased from 150° to 79°, indicating the change in the wettability of the solid surface from oleophilic to oleophobic. On the basis of the measured three-phase contact angles, the interfacial tension in the presence of the nanosheets was further calculated and was lower than the interfacial tension without the nanosheets. These interfacial phenomena can help residual oil detach from the solid surface, which contributes to the improved oil recovery performance.

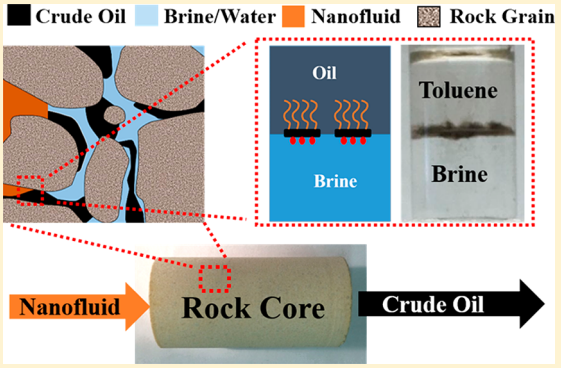

1. INTRODUCTION

The conventional production of crude oil from wells in oil fields generally has three stages. The primary stage utilizes the natural pressure difference between the wells and the reservoirs. The improved, or secondary, stage uses water flooding to continually supply reservoir energy. The enhanced, or tertiary, stage uses chemical flooding (polymer, surfactant, polymer/surfactant, alkali/polymer/surfactant, etc.) to reduce the interfacial tension and control the mobility ratio of the fluids.[1] Currently, oil recovery using chemical methods is strongly limited by the low price of crude oil, the potential pollution of underground water, and harsh reservoir conditions. Flooding with nanofluids (solutions containing dispersed nanoparticles) to improve or enhance oil recovery in reservoirs has attracted a growing amount of attention as a promising alternative to chemical flooding.[2−6] Recently, we reported a high tertiary oil recovery factor of 15.2% using a simple nanofluid (containing only nanoparticles) of graphene-based amphiphilic Janus nanosheets at a low concentration (0.01 wt % nanosheet loading), representing a substantial improvement over chemical methods in terms of a lower cost and greater environmental sustainability.[7] The high performance was possibly due to the unique interfacial behavior of these two-dimensional amphiphilic Janus nanosheets at the oil−water interface. We found that the formation of climbing and interfacial films at different conditions may lead to oil displacement, which is different from existing mechanisms for homogeneous nanoparticles, such as oil−water interfacial tension reduction,[8,9] rock surface wettability alteration,[10−12] and production of a structural disjoining force.[13−16]

Received: June 9, 2017
Revised: September 5, 2017
Accepted: September 7, 2017
Published: September 7, 2017

DOI: 10.1021/acs.iecr.7b02384
Ind. Eng. Chem. Res. XXXX, XXX, XXX−XXX

Nanofluid flooding for secondary oil recovery would be even more attractive, because it could drastically reduce costs by eliminating the need for the tertiary recovery stage and could also save large amounts of water, especially while the price of oil is low. For secondary oil recovery by simple nanofluids, Ogolo et al.[17] tested the performance of different kinds of homogeneous nanoparticles in packed-sand flooding setup, including Al_2O_3, MgO, Fe_2O_3, Ni_2O_3, ZnO, ZrO_2, SnO, and silane-treated SiO_2. In comparison with the efficiency achieved with brine flooding (3 wt % NaCl), 0.3 wt % Al_2O_3 nanofluid performed the best with an additional 5% oil recovery. Torsater et al.[18] also conducted core flooding tests with 0.01 wt % SiO_2 nanofluid in a saline environment (3 wt % NaCl) for secondary oil recovery. The averaged improved oil recovery factor was ~4%.

Here, we demonstrate that compared with brine flooding in core flooding tests, nanofluid of graphene-based amphiphilic Janus nanosheets at a concentration of 0.005 wt % increased oil recovery by up to 7.5% in a salt environment (4 wt % NaCl and 1 wt % $CaCl_2$) during the secondary stage. The obtained efficiency was the highest to the best of our knowledge at such a low concentration. In comparison with our previous application of the same nanofluid for tertiary oil recovery, although the increase is smaller than that seen using a higher nanosheet concentration (0.01 wt %) during tertiary recovery,[7] this method has unique advantages: it requires far fewer nanosheets, saves a huge amount of water, and produces oil at a higher rate, which is beneficial for fast cost recovery.

We also identified the chemical feature of the amphiphilic Janus nanosheets, which is essential for material application. Raman spectra of this two-dimensional (2D) material display two main peaks at 1342 and 1594 cm^{-1}. The blue shift of the G band of graphene oxide (GO) at 1599 cm^{-1} indicates the partial restoration of the graphitic sp^2 network. Ultraviolet−visible (UV−vis) spectroscopy reveals a main adsorption peak of the 2D nanosheet at 264 nm, indicating a red shift in comparison with GO due to the partial recovery of the π-conjugation network. Gaussian convolutions of X-ray photoelectron spectroscopy (XPS) show that the amphiphilic Janus nanosheet has an additional peak at 285.4 eV that is attributed to -C-N-, which is formed via nucleophilic substitution.

In this study, the three-phase (oil/brine or nanofluid/glass) contact angle was also measured. The adsorption of the amphiphilic Janus nanosheets at the oil−brine interface caused the change in morphology of an isolated oil droplet. In addition, the interfacial phenomenon was monitored in a toluene/brine system, in which the nanosheets spontaneously moved to the toluene−brine interface and formed a climbing film. After vigorous shaking, a strongly elastic interfacial film was generated at the interface by self-assembly, as described previously in a system of aliphatic hydrocarbon and brine.[7]

2. EXPERIMENTAL SECTION

2.1. Synthesis of Nanofluid. First, GO was synthesized by an improved chemical oxidation method.[19] First, 360 mL of concentrated sulfuric acid and 40 mL of phosphoric acid were mixed with 3 g of graphite powder for a few minutes, followed by the slow addition of 18 g of potassium permanganate ($KMnO_4$). Then, the fluid system was transferred to a water bath, maintained at 45 °C, and mildly stirred for at least 14 h. After that, the system was placed in an ice bath, and 300 mL of deionized (DI) water was poured into it. To stop the reaction, 3 mL of a 30 wt % hydrogen peroxide (H_2O_2) solution was then injected. With successive filtration and washing with 5 wt % HCl and DI water until the pH reached 5.0, the dispersion was subjected to strong sonication for 1 h for exfoliation, and solid GO was obtained after drying. Following that, a mixture of paraffin wax (80 g), GO (200 mg), and water (300 g) with 1 wt % NaCl was subjected to vigorous stirring at 1800 rpm at 75 °C and then cooled to room temperature. After being washed sequentially with NaOH (pH ~9), DI water, and ethanol, the wax particles covered with GO were dispersed in the solution of octadecylamine in absolute alcohol and stirred overnight. After being washed with ethanol, wax particles were dissolved with toluene, and amphiphilic Janus nanosheets were dried at 60 °C. The nanofluid was formed by stabilizing amphiphilic Janus nanosheets in DI water.

2.2. Characterization. The morphology of amphiphilic Janus nanosheets was examined by atomic force microscopy (AFM) (Veeco Dimensions 3000 Atomic Force Microscope). To prepare AFM specimens, samples were dispersed in DI water ultrasonically to make a diluted suspension. A drop of the suspension was placed on the silicon wafer and dried. The microscope was equipped with AFM probes from Mikromasch (HQ:NSC15/AL BS) with a tip radius of ~8 nm, a force constant of ~40 N m^{-1}, and a resonance frequency of ~325 kHz. We used the tapping mode to perform imaging with resolutions of 512 × 512. Optical microscopy (Olympus CKX41) and scanning electron microscopy (SEM) (LEO 1525, 5 kV acceleration voltage) were used to examine the surface of wax particles. Raman measurements were taken on a custom-built confocal micro-Raman setup equipped with a HORIBA iHR320 spectrometer and a Synapse CCD camera. A 532 nm continuous-wave laser was used as the excitation source. The samples of GO and amphiphilic nanosheets were placed on a Si substrate for the measurement. UV−vis spectra were recorded on a Cary 5000 UV−vis−NIR spectrophotometer. Fourier transform infrared spectroscopy (FTIR) spectra were recorded using a Nicolet iS50 FTIR spectrometer equipped with an attenuated total reflectance (ATR) accessory. A Malvern NanoSight NS300 instrument was employed to detect the particle size and concentration. The chemical states of the GO and the amphiphilic Janus nanosheets were also investigated by X-ray photoelectron spectroscopy (XPS) (Physical Electronics model 5700).

2.3. Formation of an Interfacial Film. To a glass bottle were added 2 mL of brine (4 wt % NaCl and 1 wt % $CaCl_2$) and 2 mL of toluene. Nanofluid of amphiphilic Janus nanosheets was then injected into the brine. For comparison, a GO suspension was injected into another bottle that had the same composition of brine and toluene. Both systems were then vortexed and settled to equilibrium for observation.

2.4. Oil Droplet Immersion Testing. A 1 μL portion of crude oil was deposited on a precleaned microscopic glass surface. Two cubic polydimethylsiloxane (PDMS) legs were built in a transparent cell (5.2 cm length, 5.2 cm width, and 1.6 cm height) to support the glass slide. The slide was then immersed in brine. The sessile drop was formed and dynamically monitored by a CCD camera from the side. After the crude oil drop had reached the equilibrium state, its shape was captured. A certain amount of nanofluid was then injected into the brine to achieve a nanosheet concentration of 0.005 wt %. After the equilibrium state had been achieved, the drop shape profile was obtained.

2.5. Core Flooding Tests. Crude oil samples were obtained from an oil field in China. The viscosity was 75 cP

DOI: 10.1021/acs.iecr.7b02384
Ind. Eng. Chem. Res. XXXX, XXX, XXX−XXX

at 25 °C. Nanofluid of amphiphilic Janus nanosheets at a concentration of 0.01 or 0.005 wt % was injected in a saline environment to measure the improvement in the oil recovery factor for rock cores with different permeabilities by the flooding equipment as shown in Figure S1. The flooding test was conducted sequentially with the following steps: (a) cleaning of the rock core with a Soxhlet extractor, (b) saturation of the core with brine (4 wt % NaCl and 1 wt % $CaCl_2$), (c) establishment of initial brine and oil saturation by crude oil injection until no more water was produced, (d) flooding with brine at a rate of 0.5 mL/min until no more oil (i.e., 100% water cut) was observed, (e) cleaning of the same rock core after brine flooding, (f) repeating of steps b and c, and (g) flooding with nanofluid at a rate of 0.5 mL/min until no more oil (i.e., 100% water cut) was extracted. The total injection volume of nanofluid for each flooding test was approximately 4−5 times greater than the pore volume.

3. RESULTS AND DISCUSSION

3.1. Fabrication of Amphiphilic Janus Nanosheets. The amphiphilic nanosheets were fabricated via a modified wax masking method, as depicted in Scheme 1.[19−21] It was reported

Scheme 1. Synthesis of Nanofluid Containing Graphene-Based Amphiphilic Janus Nanosheets

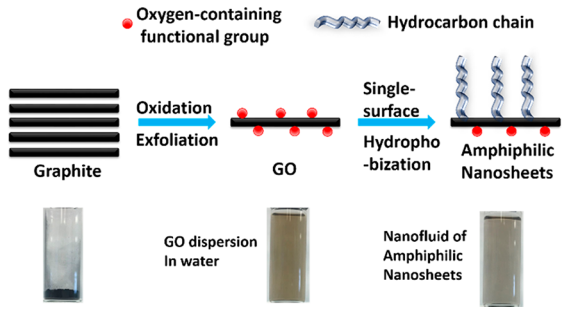

that GO alone can stabilize Pickering emulsion as solid surfactants.[22] Similarly, a wax-in-water emulsion was also formed using GO as a stabilizer. The wax particles covered by GO had varying sizes but were generally <50 μm (Figure 1a). Under SEM observation, the successful coverage of GO is

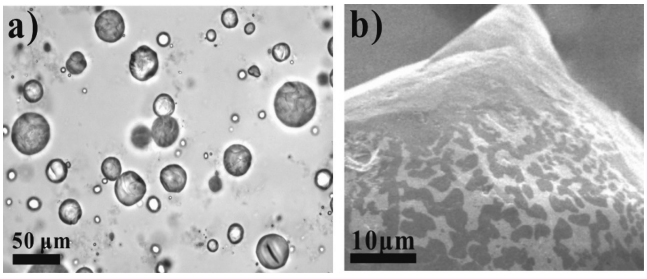

Figure 1. (a) Optical image of wax particles stabilized with GO. (b) SEM image of a wax particle surface covered with GO.

indicated by the wrinkles on the surface of wax particles (Figure 1b), which is key for both preventing wax particles from coalescing[23] and the following surface functionalization. The morphology of amphiphilic Janus nanosheets was then imaged by AFM as shown in Figure S2. GO synthesized through oxidation has an average thickness of ~1 nm,[7] which can be considered a single layer.[24,25] In comparison, the thickness of the amphiphilic Janus nanosheets changed to ~4 nm. Such a change could be attributed to the attachment of alkyl chains, which is consistent with another report.[20] The lateral dimension falls in the range of hundreds of nanometers, which was beneficial for transport in rock pores with typical sizes larger than that.[26,27]

3.2. Chemical Structure of Amphiphilic Janus Nanosheets. Natural graphite displays a G band at 1581 cm^{-1}, because of the in-phase vibration of the lattice.[28] As depicted in Figure 2a, after oxidation, the D band of GO emerges as a broad peak at 1343 cm^{-1}, resulting from the destruction of in-plane sp^2 domains and an increase in the number of defects as a result of oxidation.[29] The G band of GO shifts to 1599 cm^{-1}, due to the presence of isolated carbon double bonds vibrating at frequencies higher than that of the G band of graphite.[30] After alkyl chain conjugation, the G band is pushed to 1594 cm^{-1}, indicating the partial restoration of the graphitic sp^2 network. Previous reports showed that, after both surfaces were functionalized with alkylamine, the G band of GO shifted to 1588 cm^{-1}, much closer to that of pristine graphite.[28,31] The smaller shift in our case implied less recovery of graphitic domains, which is in agreement with the fact that only one surface of the GO was functionalized.

As shown in Figure 2b, the UV−vis spectrum of GO exhibits a strong peak at 232 nm, attributed to the $\pi-\pi^*$ transitions of graphitic C═C bonds. The shoulder adsorption at ~305 nm can be explained by the $n-\pi^*$ transitions of C═O bonds in oxygen-containing groups.[32] It can be seen that after conjugation, the absorbance standing for $\pi-\pi^*$ transitions of C═C bonds shifts to 264 nm, while the peak for $n-\pi^*$ transitions of C═O bonds can no longer be observed. The alteration in absorbance might be attributed to the increase in the π-conjugation network,[31] which is also reflected by the Raman spectra.

FTIR spectra (Figure.S3a) further demonstrated the surface functionalization of GO. Both GO and the amphiphilic nanosheets show typical peaks at 1723, 1587, and 1230 cm^{-1}, corresponding to carbonyl/carboxyl, aromatic, and epoxy vibrations, respectively.[33] In the case of the amphiphilic nanosheets, the strong asymmetric peaks at 2850 and 2925 cm^{-1}, as well as the medium peak at 1470 cm^{-1}, indicate the presence of methylene groups. Moreover, the weak signals at 1380 and 2960 cm^{-1} imply methyl groups. Those peaks are also present in the spectrum of alkylamine, which strongly confirms the successful conjugation of alkyl chains to the GO surface.

The nanofluid needs to be injected in a well-dispersed state. After settling for 30 days, neither GO nor the amphiphilic nanosheets showed observable sedimentation. The stability of the GO and amphiphilic nanosheet dispersions, both at a concentration of 0.005 wt %, was measured by a light scattering method. From the size distribution curves, it is evident that the hydrodynamic diameter of the amphiphilic nanosheets did not change much from that of GO (Figure S3b), indicating no obvious aggregation after functionalization. In addition, the modified DLVO model was built and also predicted the stable dispersion of the nanofluid.[34]

As shown in Figure 3, after Gaussian convolutions of the XPS spectrum of the C 1s region of GO with a Shirley background, it displays four fitted peaks. Binding energies of 284.8, 286.6, 287.1, and 288.7 eV correspond to the carbon skeleton (−C−C−), hydroxyl group (−C−OH), epoxy group (−C−O−C−), and carboxyl group (−O−C═O), respectively. In comparison, the XPS spectrum of the amphiphilic nanosheets exhibits a new

DOI: 10.1021/acs.iecr.7b02384
Ind. Eng. Chem. Res. XXXX, XXX, XXX−XXX

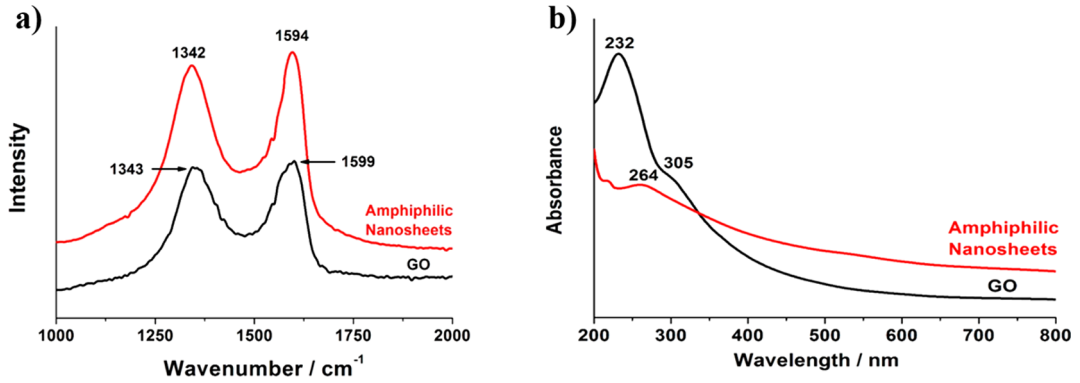

Figure 2. Chemical structure analysis of GO and graphene-based amphiphilic Janus nanosheets. (a) Raman and (b) UV−vis−NIR spectra of GO and amphiphilic Janus nanosheets.

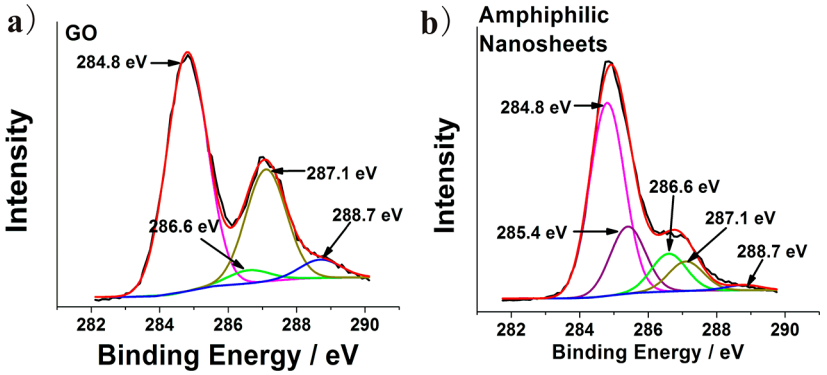

Figure 3. XPS analysis of (a) GO and (b) amphiphilic nanosheets.

peak with a binding energy of 285.4 eV, corresponding to the −C−N− bond, confirming the functionalization of GO with alkylamine.[28] In addition, the peak at ∼400 eV also demonstrated the existence of N (Figure S4). The conjugation of alkylamine to GO was mainly through nucleophilic substitution reaction on epoxy functional groups.[35,36] The ring opening of epoxy groups increased the amount of hydroxyl groups, as indicated in the area ratio change of fitted curves from GO's to that of amphiphilic Janus nanosheets.

3.3. Interfacial Behavior. Previously, we demonstrated that amphiphilic Janus graphene-based nanosheets were able to form climbing film and interfacial film in a heptane/brine system. Heptane is a representative aliphatic hydrocarbon with an interfacial tension to water higher than that of crude oil.[37,38] Considering that the crude oil in reservoirs contains both aliphatic and aromatic hydrocarbons, we decided to study the behavior of nanosheets in a toluene/brine system, because the toluene/brine interfacial tension is much closer to that of the crude oil/brine system.[39] As shown in Figure S5, GO precipitated after injection into the toluene/brine system. In contrast, the amphiphilic nanosheets formed an interfacial film between toluene and brine even after vigorous shaking. Attachment of small pieces of amphiphilic interfacial film was observed on the hydrophilic glass surface in the toluene phase, appearing as black dots. Upon introduction of a glass rod, the interfacial film of amphiphilic nanosheets did not break, exhibiting resistance to the intrusion (Figure 4). After the glass rod was removed, the interfacial film recovered and remained intact, demonstrating its elasticity. This film was also recovered even after being seriously disrupted, as described previously in a heptane/brine system.[7]

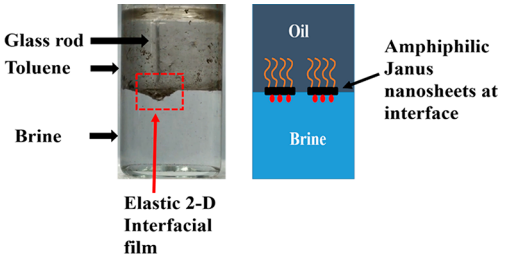

Figure 4. Interfacial film of amphiphilic Janus nanosheets at the toluene−brine interface responding to the intrusion of a glass rod (left) and schematic illustration of amphiphilic nanosheets at the oil−brine interface (right).

Our nanofluid with 0.005 wt % nanoheets has a surface tension of ∼36.8 mN/m, much lower than those of common nanofluids such as TiO_2, Al_2O_3, and SiO_2 of ∼70 mN/m (Table S1).[40] To further investigate the interfacial behavior of the amphiphilic nanosheets, we first measured the interfacial tension between crude oil and brine, γ_{OL}, using the pendent drop method. The images of crude oil droplets were recorded by dataphysics with a model OCA 15EC instrument as shown in Figure 5a−c from three measurements under the same conditions. The shape of oil droplets was balanced between the buoyant force and oil/brine interfacial tension. Mathematically, it gives[41]

$$\gamma_{OL} = \Delta\rho g R_0^2/\beta \quad (1)$$

where $\Delta\rho$ is the difference in density between the oil and brine phases, g is the gravitational acceleration, R_0 is the radius of curvature at the drop apex, and β is the shape factor.

DOI: 10.1021/acs.iecr.7b02384
Ind. Eng. Chem. Res. XXXX, XXX, XXX−XXX

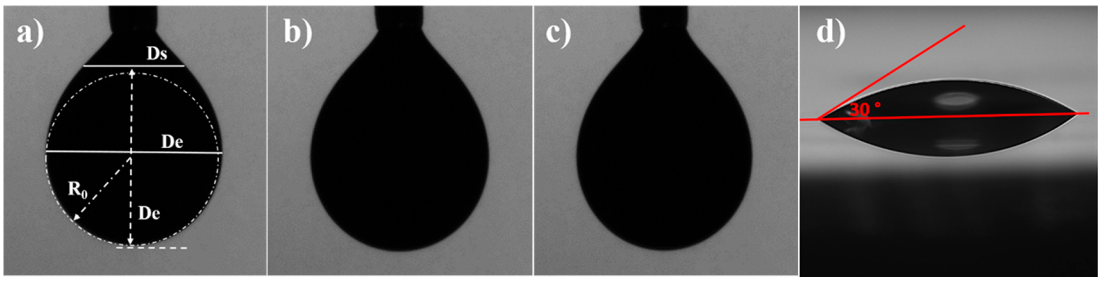

Figure 5. (a–c) Shape of crude oil in brine from three pendent drop measurements. (d) Contact angle of water on a graphene-based amphiphilic Janus nanosheet-coated glass surface.

Meanwhile, R_0 and β can be calculated from two parameters, the equatorial diameter of drop (D_e) and D_s, the diameter located distance D_e vertically from the vertex. Shape factor β was found[41]

$$\beta = 0.12836 - 0.7577\frac{D_s}{D_e} + 1.7713\left(\frac{D_s}{D_e}\right)^2 - 0.5426\left(\frac{D_s}{D_e}\right)^3 \quad (2)$$

For $0.1 < \beta < 0.5$, R_0 was calculated from the following equation[41]

$$\frac{D_e}{2R_0} = 0.9987 + 0.1971\beta - 0.0734\beta^2 + 0.34708\beta^3 \quad (3)$$

where D_e and D_s/D_e were extracted from the shape of the droplets. The averaged values from three measurements were 1.89 mm and 0.55, respectively. Therefore, shape factor β was calculated to be 0.1572, while R_0 was 0.9182 mm. With the knowledge of the density difference, $\Delta\rho = (1.035 - 0.845)$ g/cm^3 = 0.19 g/cm^3, the interfacial tension between crude oil and brine was calculated to be ~10.0 mN/m, which is within the reasonable range of the previous reports.[38]

To calculate the oil–brine interfacial tension in the presence of nanosheets, we performed the following procedures. First, we placed a 1 μL brine droplet on the untreated glass slide and observed a contact angle (defined as the angle between the glass surface and brine phase) of 42°. Young's equation can be expressed as

$$\gamma_{SL} + \gamma_L \cos\theta = \gamma_S \quad (4)$$

where γ_{SL} is the interfacial tension between the untreated glass slide and brine, γ_L is the surface tension of brine, which is ~72 mN/m, θ is the contact angle at equilibrium, and γ_S is the surface tension of the glass slide.

After we coated the glass slide with our amphiphilic Janus nanosheets (AJN) with the hydrophilic side facing upward, we also placed a 1 μL brine droplet on the coated area and observed a contact angle of 30°. Similarly, Young's equation can be expressed as

$$\gamma_{SNL} + \gamma_L \cos\theta_{AJN} = \gamma_S \quad (5)$$

where γ_{SNL} is interfacial tension between the AJN-coated glass slide and brine. Both γ_L and γ_S remain unchanged. The change in the solid–liquid interfacial tension can be defined as

$$\gamma_{SL} - \gamma_{SNL} = 8.85\ \text{mN/m} \quad (6)$$

The interfacial tension between the solid and brine decreased because the coating of AJN made the glass surface more hydrophilic, thus decreasing the contact angle of brine on the glass slide.

To calculate the oil–brine interfacial tension in the presence of nanosheets, a crude oil droplet was immobilized under a glass slide and pressed into brine to mimic the reservoir condition (Figure 6a). For the three-phase system (oil/water/solid phases), right after the glass slide was immersed in brine, the contact angle (defined as the angle between the glass surface and brine phase) was 150° (Figure 6b) and Young's equation can be expressed as

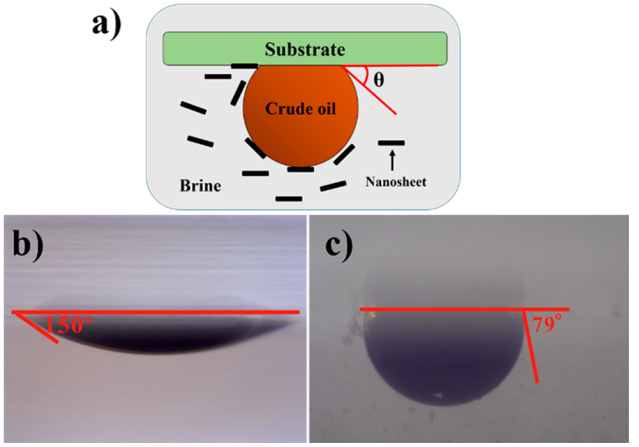

Figure 6. (a) Side-view illustration of a crude oil droplet under the glass slide in brine. Side-view images of a crude oil droplet under a glass slide in (b) brine and (c) nanofluid and brine.

$$\gamma_{SO} + \gamma_{OL}|\cos 150°| = \gamma_{SL} \quad (7)$$

where γ_{SO} is the interfacial tension between the oil and glass slide, γ_{SL} is the interfacial tension between the brine and glass slide, and γ_{OL} is the interfacial tension between oil and brine. After the nanofluid was injected, gradually the nanosheets moved to the glass surface in the oil/brine/glass three-phase region, decreasing γ_{SL} as described above.[16] Meanwhile, the nanosheets would also move to the oil–brine interface, reducing oil–brine interfacial tension γ_{OL}. Eventually, the oil droplet shape changed and the contact was measured as 79° at the equilibrium (Figure 6c). Equation 4 can be modified as

$$\gamma_{SO} = \gamma_{SNL} + \gamma_{ONL}\cos 79° \quad (8)$$

where γ_{SNL} is the interfacial tension between brine and the AJN-attached glass slide, γ_{OLN} represents the interfacial tension between oil and brine with nanosheets, and γ_{SO} remained unchanged. Via combination of eqs 7 and 8, γ_{OLN} can be derived as

DOI: 10.1021/acs.iecr.7b02384
Ind. Eng. Chem. Res. XXXX, XXX, XXX–XXX

$$\gamma_{ONL} \cos 79° = \gamma_{SL} - \gamma_{SNL} - \gamma_{OL}|\cos 150°| \quad (9)$$

Via combination of eq 6, γ_{ONL} was calculated to be 1.0 mN/m.

From the calculations mentioned above, it is evident that the nanosheets altered the glass surface wettability from oleophilic to oleophobic by spreading into the three-phase region. Nanosheets also attached to the oil droplet surface to reduce the oil−brine interfacial tension. Both factors contributed to the evolution of the shape of the oil droplet, which led to detachment of oil from the solid surface.[42,43] Under stronger hydrodynamic conditions in reservoirs, the formation of the nanosheet interfacial film may further decrease the oil−brine interfacial tension.

3.4. Oil Recovery Efficiency. The oil recovery factor was calculated as the ratio of the volume of crude oil produced by flooding with brine water or nanofluid to the original volume of injected oil. Four human-made sandstone rock cores were chosen; their corresponding physical properties are listed in Table 1. The liquid permeabilities of samples 1 and 2 were relatively low, whereas those of samples 3 and 4 were higher. As shown in Table 2, all of the tests showed that nanofluid flooding was more efficient than brine flooding. The efficiency of nanofluid flooding is due to the amphiphilicity of the nanosheets, which, with the proper underground hydrodynamic conditions, may reduce the interfacial tension, help to detach oil from the rock surface by forming a climbing film, and displace the oil by generating a relatively strong, elastic, interfacial film.[7]

Table 1. Physical Properties of the Rock Cores Used for Flooding Tests

rock core	length (cm)	diameter (cm)	porosity (%)	average liquid permeability (mD)	pore volume (cm^3)
1	4.040	2.526	21.55	43.29	4.363
2	4.035	2.510	26.26	56.58	5.243
3	3.970	2.547	25.44	126.6	5.146
4	3.850	2.550	24.98	136.9	4.912

Table 2. Improvements in the Oil Recovery Factor Achieved by Flooding with Different Nanofluid Concentrations

rock core	nanofluid concentration (wt %)	oil recovery factor for brine flooding (%)	oil recovery factor for nanofluid flooding (%)	improved oil recovery factor (%)
1	0.005	67.5	75.0	7.5
2	0.01	63.0	68.8	5.8
3	0.005	64.0	70.5	6.5
4	0.01	69.1	73.8	4.7

For both low- and high-liquid permeability rock cores, the oil recovery performance was better at 0.005 wt % than at 0.01 wt %. The results are different from those of nanofluid flooding for tertiary oil recovery, which produced the best results at a concentration of 0.01 wt %.[7] The difference could be explained by the less isolated residual oil phase in the secondary recovery stage. In the tertiary stage, after prolonged water flooding, the water becomes the continuous phase in the reservoir and dominantly occupies most of the volume of the rock pores. The oil phase is either trapped in dead-end pores, which cannot be extracted even in the tertiary stage, or attached to the rock surface in a scattered and isolated state. At the secondary stage, however, the oil is often the continuous phase. As a result, the area of interface between the oil and the water is larger at the tertiary stage and requires more amphiphilic Janus nanosheets to reduce the interfacial tension. The excess amphiphilic Janus nanosheets would either concentrate at the oil−water interface or further extend the climbing film. Because the main limitation to oil recovery at the secondary stage is insufficient reservoir energy or pressure, the excess nanosheets might increase the flooding resistivity, leading to a lower oil recovery factor. Therefore, the nanofluid at 0.005 wt % performs better. We intentionally recorded the decrease in pressure in single-phase fluid (only nanofluid) flow for two similar rock cores with ∼50 mD permeabilities after injection of 0.5 pore volume (PV) because the nanosheets were present in the rock core in certain amounts. From Figure 7, we can find that the decrease in pressure with 0.01 wt % nanosheets was larger than that found at 0.005 wt %, which indicated higher flooding resistivity when more nanosheets existed.

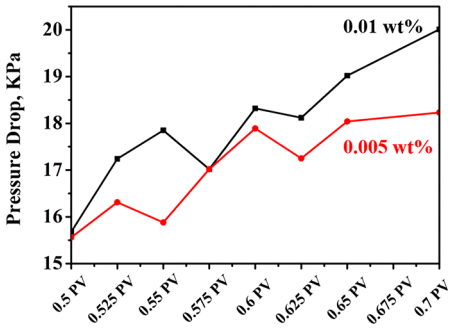

Figure 7. Pressure drop transient profile by nanofluid flooding during injection from 0.5 to 0.7 PV.

4. CONCLUSIONS

In conclusion, nanofluid containing graphene-based amphiphilic Janus nanosheets at an ultralow concentration can improve secondary oil recovery by 7.5%, which is superior to the performance of homogeneous nanoparticles even at higher concentrations. The successful exfoliation and functionalization of graphite give the nanosheets an amphiphilic property and a Janus structure, resulting in the unique interfacial behavior in a hydrocarbon/brine system that is responsible for effective oil displacement. In contrast to our previous method for tertiary oil recovery, the use of the nanofluid at a lower concentration in secondary recovery eliminates the need for the tertiary stage, which can significantly reduce the overall cost to compensate for the loss of oil recovery efficiency compared with the use of the nanofluid at the tertiary stage. Thus, our results provide the petroleum industry with an important alternative to consider when making decisions about the timing of oil recovery implementation to maximize operating results in the current economic environment.

■ ASSOCIATED CONTENT

Supporting Information

The Supporting Information is available free of charge on the ACS Publications website at DOI: 10.1021/acs.iecr.7b02384.

Core flooding machine used in the experiments, morphology of graphene-based amphiphilic Janus nanosheets imaged by AFM, FTIR spectra and particle size distribution, N 1s and O 1s XPS spectra of graphene-based amphiphilic Janus nanosheets, behavior of GO-

DOI: 10.1021/acs.iecr.7b02384
Ind. Eng. Chem. Res. XXXX, XXX, XXX−XXX

and graphene-based amphiphilic Janus nanosheets in a toluene/brine system, and surface tensions of common nanofluids (PDF)

AUTHOR INFORMATION

Corresponding Authors

*E-mail: zren@uh.edu.
*E-mail: yangzhaozhong@swpu.edu.cn.

ORCID

Jingyi Zhu: 0000-0003-1973-5632
Zhuan Zhu: 0000-0003-4377-9053
Jiming Bao: 0000-0002-6819-0117
Zhifeng Ren: 0000-0001-8233-3332

Author Contributions

D.L. and F.W. contributed equally to this work.

Funding

This work was supported by the U.S. Department of Energy under Contract DE-SC0010831.

Notes

The authors declare no competing financial interest.

ACKNOWLEDGMENTS

We thank Prof. Dong Cai (University of Houston) for providing NanoSight NS300 for particle size measurements.

REFERENCES

(1) Liu, S. H.; Zhang, D. L.; Yan, W.; Puerto, M.; Hirasaki, G. J.; Miller, C. A. Favorable attributes of alkaline-surfactant-polymer flooding. *SPE Journal* **2008**, *13* (1), 5−16.

(2) Hendraningrat, L.; Li, S. D.; Torsæter, O. A coreflood investigation of nanofluid enhanced oil recovery. *J. Pet. Sci. Eng.* **2013**, *111*, 128−138.

(3) Torsaeter, O.; Li, S.; Hendraningrat, L. Enhancing Oil Recovery of Low-Permeability Berea Sandstone through Optimised Nanofluids Concentration. SPE Enhanced Oil Recovery Conference, July 2−4, Kuala Lumpur, Malaysia; Society of Petroleum Engineers: Richardson, TX, 2013.

(4) Hendraningrat, L.; Torsaeter, O. Metal oxide-based nanoparticles: revealing their potential to enhance oil recovery in different wettability systems. *Appl. Nanosci.* **2015**, *5* (2), 181−199.

(5) Zargartalebi, M.; Kharrat, R.; Barati, N. Enhancement of surfactant flooding performance by the use of silica nanoparticles. *Fuel* **2015**, *143*, 21−27.

(6) Cheraghian, G.; Hendraningrat, L. A review on applications of nanotechnology in the enhanced oil recovery part A: effects of nanoparticles on interfacial tension. *Int. Nano Lett.* **2016**, *6* (1), 129−138.

(7) Luo, D.; Wang, F.; Zhu, J. Y.; Cao, F.; Liu, Y.; Li, X. G.; Willson, R. C.; Yang, Z. Z.; Chu, C. W.; Ren, Z. F. Nanofluid of graphene-based amphiphilic Janus nanosheets for tertiary or enhanced oil recovery: High performance at low concentration. *Proc. Natl. Acad. Sci. U. S. A.* **2016**, *113* (28), 7711−7716.

(8) Binks, B. P. Particles as surfactants - similarities and differences. *Curr. Opin. Colloid Interface Sci.* **2002**, *7* (1−2), 21−41.

(9) Zhang, H.; Nikolov, A.; Wasan, D. Enhanced Oil Recovery (EOR) Using Nanoparticle Dispersions: Underlying Mechanism and Imbibition Experiments. *Energy Fuels* **2014**, *28* (5), 3002−3009.

(10) Giraldo, J.; Benjumea, P.; Lopera, S.; Cortes, F. B.; Ruiz, M. A. Wettability Alteration of Sandstone Cores by Alumina-Based Nanofluids. *Energy Fuels* **2013**, *27* (7), 3659−3665.

(11) Karimi, A.; Fakhroueian, Z.; Bahramian, A.; Pour Khiabani, N.; Darabad, J. B.; Azin, R.; Arya, S. Wettability Alteration in Carbonates using Zirconium Oxide Nanofluids: EOR Implications. *Energy Fuels* **2012**, *26* (2), 1028−1036.

(12) Lim, S.; Horiuchi, H.; Nikolov, A. D.; Wasan, D. Nanofluids Alter the Surface Wettability of Solids. *Langmuir* **2015**, *31* (21), 5827−5835.

(13) Wasan, D. T.; Nikolov, A. D. Spreading of nanofluids on solids. *Nature* **2003**, *423*, 156−159.

(14) Kondiparty, K.; Nikolov, A. D.; Wasan, D.; Liu, K. L. Dynamic Spreading of Nanofluids on Solids. Part I: Experimental. *Langmuir* **2012**, *28* (41), 14618−14623.

(15) Liu, K. L.; Kondiparty, K.; Nikolov, A. D.; Wasan, D. Dynamic Spreading of Nanofluids on Solids Part II: Modeling. *Langmuir* **2012**, *28* (47), 16274−16284.

(16) Wasan, D.; Nikolov, A.; Kondiparty, K. The wetting and spreading of nanofluids on solids: Role of the structural disjoining pressure. *Curr. Opin. Colloid Interface Sci.* **2011**, *16* (4), 344−349.

(17) Ogolo, N. A.; Olafuyi, O. A.; Onyekonwu, M. O. Enhanced Oil Recovery Using Nanoparticles. SPE Saudi Arabia Section Technical Symposium and Exhibition, April 8−11, Al-Khobar, Saudi Arabia; Society of Petroleum Engineers: Richardson, TX, 2012.

(18) Torsater, O.; Engeset, B.; Hendraningrat, L.; Suwarno, S. Improved Oil Recovery by Nanofluids Flooding: An Experimental Study. SPE Kuwait International Petroleum Conference and Exhibition, December 10−12, Kuwait City, Kuwait; Society of Petroleum Engineers: Richardson, TX, 2012.

(19) Marcano, D. C.; Kosynkin, D. V.; Berlin, J. M.; Sinitskii, A.; Sun, Z. Z.; Slesarev, A.; Alemany, L. B.; Lu, W.; Tour, J. M. Improved Synthesis of Graphene Oxide. *ACS Nano* **2010**, *4* (8), 4806−4814.

(20) Wu, H.; Yi, W. Y.; Chen, Z.; Wang, H. T.; Du, Q. G. Janus graphene oxide nanosheets prepared via Pickering emulsion template. *Carbon* **2015**, *93*, 473−483.

(21) Hong, L.; Jiang, S.; Granick, S. Simple method to produce Janus colloidal particles in large quantity. *Langmuir* **2006**, *22* (23), 9495−9499.

(22) He, Y. Q.; Wu, F.; Sun, X. Y.; Li, R. Q.; Guo, Y. Q.; Li, C. B.; Zhang, L.; Xing, F. B.; Wang, W.; Gao, J. P. Factors that Affect Pickering Emulsions Stabilized by Graphene Oxide. *ACS Appl. Mater. Interfaces* **2013**, *5* (11), 4843−4855.

(23) Xu, F. G.; Fang, Z. H.; Yang, D. G.; Gao, Y.; Li, H. M.; Chen, D. Y. Water in Oil Emulsion Stabilized by Tadpole-like Single Chain Polymer Nanoparticles and Its Application in Biphase Reaction. *ACS Appl. Mater. Interfaces* **2014**, *6* (9), 6717−6723.

(24) Dikin, D. A.; Stankovich, S.; Zimney, E. J.; Piner, R. D.; Dommett, G. H. B.; Evmenenko, G.; Nguyen, S. T.; Ruoff, R. S. Preparation and characterization of graphene oxide paper. *Nature* **2007**, *448*, 457−460.

(25) Peng, L.; Xu, Z.; Liu, Z.; Wei, Y. Y.; Sun, H. Y.; Li, Z.; Zhao, X. L.; Gao, C. An iron-based green approach to 1-h production of single-layer graphene oxide. *Nat. Commun.* **2015**, *6*, 5716.

(26) Doyen, P. M. Permeability, Conductivity, And Pore Geometry Of Sandstone. *J. Geophys. Res.* **1988**, *93* (B7), 7729−7740.

(27) Nelson, P. H. Pore-throat sizes in sandstones, tight sandstones, and shales. *AAPG Bull.* **2009**, *93*, 329−340.

(28) Li, W. J.; Tang, X. Z.; Zhang, H. B.; Jiang, Z. G.; Yu, Z. Z.; Du, X. S.; Mai, Y. W. Simultaneous surface functionalization and reduction of graphene oxide with octadecylamine for electrically conductive polystyrene composites. *Carbon* **2011**, *49* (14), 4724−4730.

(29) Samanta, S.; Singh, S.; Sahoo, R. R. Simultaneous chemical reduction and surface functionalization of graphene oxide for efficient lubrication of steel-steel contact. *RSC Adv.* **2015**, *5* (76), 61888−61899.

(30) Moon, I. K.; Lee, J.; Ruoff, R. S.; Lee, H. Reduced graphene oxide by chemical graphitization. *Nat. Commun.* **2010**, *1*, 73.

(31) Choudhary, S.; Mungse, H. P.; Khatri, O. P. Dispersion of alkylated graphene in organic solvents and its potential for lubrication applications. *J. Mater. Chem.* **2012**, *22* (39), 21032−21039.

(32) Guardia, L.; Villar-Rodil, S.; Paredes, J. I.; Rozada, R.; Martinez-Alonso, A.; Tascón, J. M. D. UV light exposure of aqueous graphene oxide suspensions to promote their direct reduction, formation of graphene-metal nanoparticle hybrids and dye degradation. *Carbon* **2012**, *50* (3), 1014−1024.

DOI: 10.1021/acs.iecr.7b02384
Ind. Eng. Chem. Res. XXXX, XXX, XXX−XXX

(33) Acik, M.; Lee, G.; Mattevi, C.; Chhowalla, M.; Cho, K.; Chabal, Y. J. Unusual infrared-absorption mechanism in thermally reduced graphene oxide. *Nat. Mater.* **2010**, *9*, 840−845.
(34) Luo, D.; Wang, F.; Alam, M. K.; Yu, F.; Mishra, I. K.; Bao, J.; Willson, R. C.; Ren, Z. F. Colloidal stability of graphene-based amphiphilic Janus nanosheet fluid. *Chem. Mater.* **2017**, *29* (8), 3454−3460.
(35) Tan, M. T.; Liu, X.; Li, W.; Li, H. X. Enhancing Sorption Capacities for Copper(II) and Lead(II) under Weakly Acidic Conditions by L-Tryptophan-Functionalized Graphene Oxide. *J. Chem. Eng. Data* **2015**, *60* (5), 1469−1475.
(36) Dreyer, D. R.; Park, S.; Bielawski, C. W.; Ruoff, R. S. The chemistry of graphene oxide. *Chem. Soc. Rev.* **2010**, *39*, 228−240.
(37) Zeppieri, S.; Rodriguez, J.; López de Ramos, A. L. Interfacial tension of alkane plus water systems. *J. Chem. Eng. Data* **2001**, *46* (5), 1086−1088.
(38) Buckley, J. S.; Fan, T. G. Crude oil/brine interfacial tensions. *Petrophysics* **2007**, *48* (3), 175−185.
(39) Saien, J.; Akbari, S. Interfacial tension of toluene plus water plus sodium dodecyl sulfate from (20 to 50) degrees C and pH between 4 and 9. *J. Chem. Eng. Data* **2006**, *51* (5), 1832−1835.
(40) Bhuiyana, M. H. U.; Saidura, R.; Amalinaa, M. A.; Mostafizura, R. M.; Islamc, A. K. M. S. Effect of nanoparticles concentration and their sizes on surface tension of nanofluids. *Procedia Eng.* **2015**, *105*, 431−437.
(41) Hansen, F. K.; Rødsrud, G. Surface tension by pendant drop: I. A fast standard instrument using computer image analysis. *J. Colloid Interface Sci.* **1991**, *141* (1), 1−9.
(42) dos Santos, R. G.; Mohamed, R. S.; Bannwart, A. C.; Loh, W. Contact angle measurements and wetting behavior of inner surfaces of pipelines exposed to heavy crude oil and water. *J. Pet. Sci. Eng.* **2006**, *51* (1−2), 9−16.
(43) Mohammed, M.; Babadagli, T. Wettability alteration: A comprehensive review of materials/methods and testing the selected ones on heavy-oil containing oil-wet systems. *Adv. Colloid Interface Sci.* **2015**, *220*, 54−77.

DOI: 10.1021/acs.iecr.7b02384
Ind. Eng. Chem. Res. XXXX, XXX, XXX−XXX